PERGAMON

Journal of Structural Geology 24 (2002) 1281–1297

JOURNAL OF STRUCTURAL GEOLOGY

www.elsevier.com/locate/jstrugeo

Oxygen isotope record of fluid–rock–SiO_2 interaction during Variscan progressive deformation and quartz veining in the meta-volcanosediments of Belle-Ile (Southern Brittany)

Bernhard Schulz[a,*], Claude Audren[b], Claude Triboulet[c]

[a]*Institut für Mineralogie der TU Bergakademie, Brennhausgasse 14, D-09596 Freiberg/Sachsen, Germany*
[b]*Géosciences Rennes, Laboratoire de Tectonique, C.N.R.S. U.P.R. 4661, F-35042 Rennes Cedex, France*
[c]*Laboratoire de Pétrologie Minéralogique, C.N.R.S. U.R.A. 736, Université Pierre et Marie Curie, 4 place Jussieu, F-75252 Paris Cedex 05, France*

Received 30 January 2001; revised 24 September 2001; accepted 9 October 2001

Abstract

Belle-Ile in the South Armorican Domain is composed of Palaeozoic volcano-detrital sequences with sericite phyllites and porphyroids. Fine-banded and folded meta-tuffites, microquartzites and graphitic quartzites occur in the basal part at Plage de Bordardoué. Phengite compositions constrain that Variscan metamorphism did not exceed 430 °C/4.5 kbar. Four generations (1–4) of centimeter-thick quartz veins were precipitated during Variscan progressive deformation and recorded changing fluid compositions. Values of 26‰ $\delta^{18}O_{SMOW}$ in vein 1 quartz exceed high $\delta^{18}O_{SMOW}$ in the host rocks. Decrease of quartz $\delta^{18}O_{SMOW}$ from margins to centers can be observed from the syntaxial veins. Younger veins 4 have lower $\delta^{18}O$. Their inclusions indicate lower salinities and traces of CH_4 in the fluid when compared with veins 1. Veins 1 were overprinted by shearing and fissuring. Subgrain rotation recrystallization occurred along briquette structures and subgrain boundaries. The initial isotope values have been preserved. Larger domains with small-grained quartz can be identified by lower values of $\delta^{18}O$. Homogeneous isotopic compositions are found in hinges of folded veins 2 with grain boundary migration recrystallization. The small-scale oxygen isotope variations and the changing fluid compositions point to a locally hosted fluid system with a limited contribution of meteoric water during multiphase deformation and vein formation.

Keywords: Veins; Progressive deformation; Oxygen isotopes; Fluid; Meta-volcanosediments; South Armorican Domain

1. Introduction

Quartz veins are geological features giving evidence of past fluid flow in rocks. The vein geometry and structure provide information about vein formation and deformation, and when combined with fluid inclusion and oxygen isotope studies, a changing of fluid–rock interaction parameters during geological time and space can be revealed (Rumble, 1977, 1994; Cox and Etheridge 1989; Fisher and Byrne, 1990). Stable isotope and fluid inclusion studies on veins and their host rocks allow the evaluation of the regional scales of the fluid systems, of their character, open or closed, and of the main fluid transfer and driving mechanisms (Kerrich, 1986; Ferry, 1992; O'Hara and Haak, 1992; Dipple and Ferry, 1992a; Oliver et al., 1993; Slater et al., 1994; Henderson and McCaig, 1996). Dependent on the scale, a discrimination among closed systems, fractured and unfractured, and open systems, pervasive or channelized, with wallrock interaction or not, has been proposed by Oliver (1996).

Many studies on veins consider a regional scale of kilometer or tens of kilometers. Some attention has been dedicated to isotope variations in the centimeter- or millimeter-scale within single veins and the interpretation of such observations (Rye and Bradbury, 1988; Kirschner et al., 1993; Slater et al., 1994). Furthermore, the small-scale changes and second order effects upon the stable isotope systems during deformational processes in such veins are poorly known (Kirschner et al., 1995). In the Variscan low-grade meta-volcanosedimentary sequence of Belle-Ile-en-mer in southern Brittany (France), several generations of quartz veins crystallized during successive phases or steps of bulk rock deformation. The structural and microstructural evolution of the veins together with the related variations of oxygen isotope values and the fluid-inclusion compositions in quartz are described. This allowed the evaluation of the dimension, the changing compositions, and the provenance of the fluid(s) during a progressive deformation.

* Corresponding author. Fax: +49-09131-852-9295.
E-mail address: bschulz@geol.uni-erlangen.de (B. Schulz).

0191-8141/02/$ - see front matter
PII: S0191-8141(01)00135-3

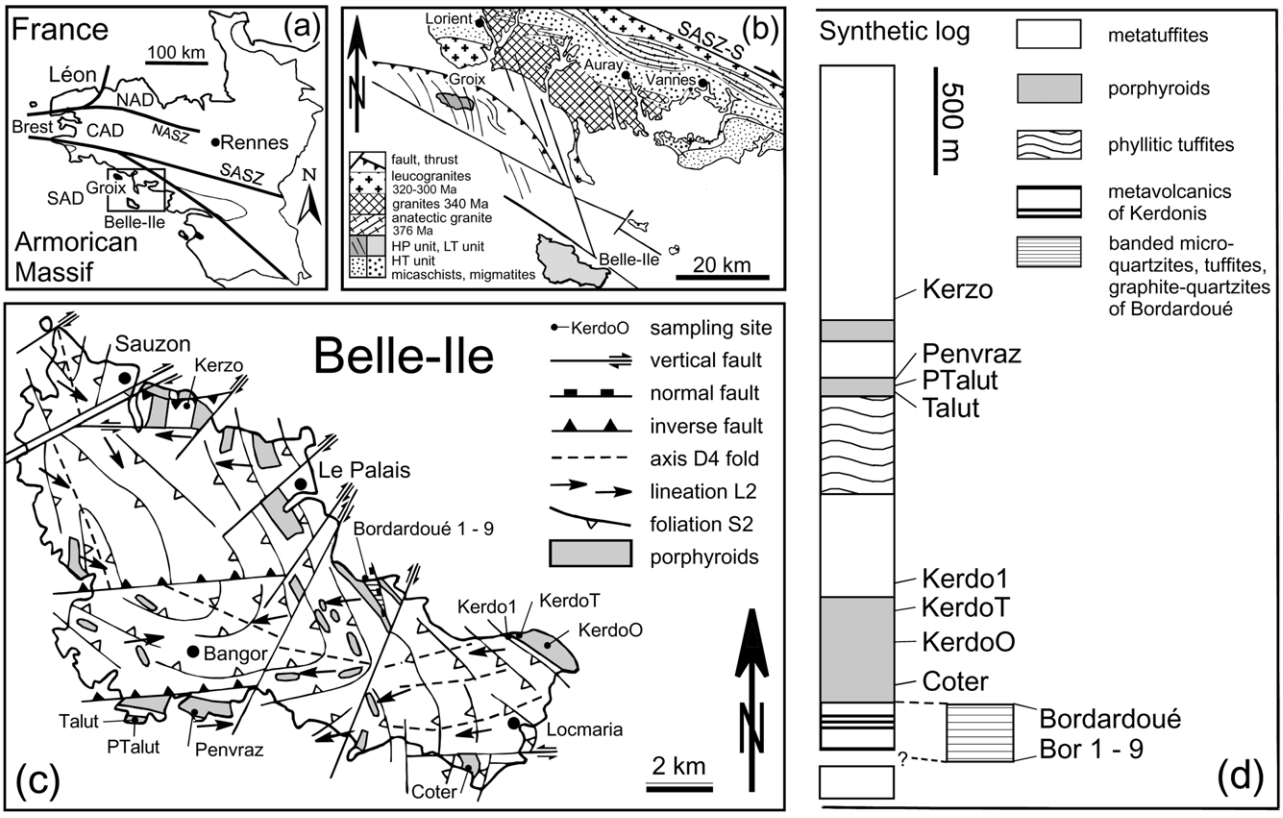

Fig. 1. Regional geology in the Armorican Massif, western France. (a) Tectonic subdivison. (b) Geological map of the South Armorican Domain. (c) Structural geology in the island of Belle-Ile-en-Mer (Audren, 1987) and sample locations. CAD = Central Armorican Domain; NAD = North Armorican Domain; SAD = South Armorican Domain; NASZ = North Armorican shear zone; SASZ-S = South Armorican shear zone (southern branch). (d) Synthetic lithological column of the Belle-Ile volcano-sedimentary sequence and positions of sampling sites.

2. Regional geology

The island Belle-Ile-en-mer in the South Armorican Domain of the Armorican Massif (Fig. 1a–c) is composed of a 3000-m-thick volcanic and volcano-detrital sequence of presumably Lower to Middle Palaeozoic (Ordovician?) age (Audren and Plaine, 1986). Monotonous sericite phyllites (meta-tuffites) and porphyroids (former ignimbrites) dominate the lithological sequence; graphite quartzites, graphite phyllite, phyllitic tuffites, former keratophyric tuffs and chert are found at its base (Fig. 1d). Apart from rare and local late dolomitization (dolomitic tuffites), carbonate rocks do not occur. An intermediate tectonostratigraphic position of this Belle-Ile volcano-sedimentary sequence in the South Armorican crustal pile, above the micaschists and migmatites of the Variscan high-temperature zone on the mainland, and beneath the high-pressure low-temperature blueschist klippe of the Ile de Groix has been deduced from regional geological and geophysical studies (Audren, 1987; Audren et al., 1993).

Complex polyphase Variscan deformation with shearing and folding affected the volcano-sedimentary rocks (Audren, 1987; Audren and Gorre, 1995). An early deformation D1 was characterized by a top-to-E directed tectonic transport, which changed into a top-to-W directed tectonic transport subparallel to the stretching lineation during a later deformation D2. Sheath-like and isoclinal folds F2, the main foliation S2 and the W-to-NW directed stretching lineation L2 were formed during D2. The foliation S2 is penetrative throughout the whole sequence and mylonitic microstructures (F2-microfolds, mantled porphyroclasts, mica fish, strain fringes of fibrous quartz around pyrite) give evidence of high strain during D1 and D2. S2 and L2 were then deformed in F3 folds of various geometries. F3 folds are sometimes accompanied by an axial-plane foliation S3. At Bordardoué plage (Figs. 1c, 3a and 6a), monoclinal F3 folds exhibit a spectacular development of different fold propagation stages within a layered lithology (Audren and Gorre, 1995). Deformation D4 led to a kilometer-scale synformal structure F4 with a NW–SE to W–E directed fold axis (Fig. 1c). The deformation D5 is characterized by kink folds F5 and faults. Inverse faults occur at Kerzo and to the south and the north of Bangor. Dextral strike-slip displacement is observed in NE–SW trending vertical faults. W–E trending vertical faults show sinistral displacement. Normal faults croup out at Bordardoué plage (Figs. 1c and 3a). The deformation phases have been associated with early-Variscan or Devonian shearing (D1, D2), followed by late-Variscan (Carboniferous) D3–D4–D5 transpressive dextral shearing (Audren, 1987).

3. Conditions of metamorphism

Temperatures and pressures of the syndeformational Variscan metamorphism have not yet been quantified. A low pressure–low temperature evolution has been suggested from petrographical observations (Audren, 1984, 1987). Samples from porphyroids (KerdoO, Coter, Penvraz, PTal5, Talut), phyllitic tuffites (Kerdo1, KerdoT), a phyllite (Kerzo) and a quartzite (Bor) represent bulk rock compositional variations within the silicic volcano-sedimentary sequence (Fig. 1c). The major element compositions range from SiO_2 57.1–74 (in wt%), Na_2O 0.08–2.29, K_2O 1.64–10.61, FeO^{tot} 0.92–6.96 and MgO 0.21–2.38 (all in wt%). Linear correlations of main element abundances are attributed to magmatic fractionation processes. In porphyroids with magmatic K-feldspar, a recrystallization to metamorphic K-feldspar with similar composition is observed in tension cracks and pressure shadows (Fig. 2a). Metamorphic white mica occurs along the main foliation S2 and in domains with a crenulated foliation S1 (Fig. 2b). The syn-S2 greenschist facies mineral assemblages involve in dependence on the bulk composition (+opaques + TiO_2-bearing phases):

1. Phengite + quartz (sample Bor),
2. Phengite + K-feldspar + quartz (samples Talut, PTal5, KerdoO),
3. Phengite + K-feldspar + albite + quartz (samples Coter, Penvraz),
4. Phengite + chlorite + albite + quartz (sample Kerzo),
5. Phengite + chlorite + K-feldspar + quartz (sample KerdoT),
6. Phengite + chlorite + K-feldspar + albite + quartz (sample Kerdo1).

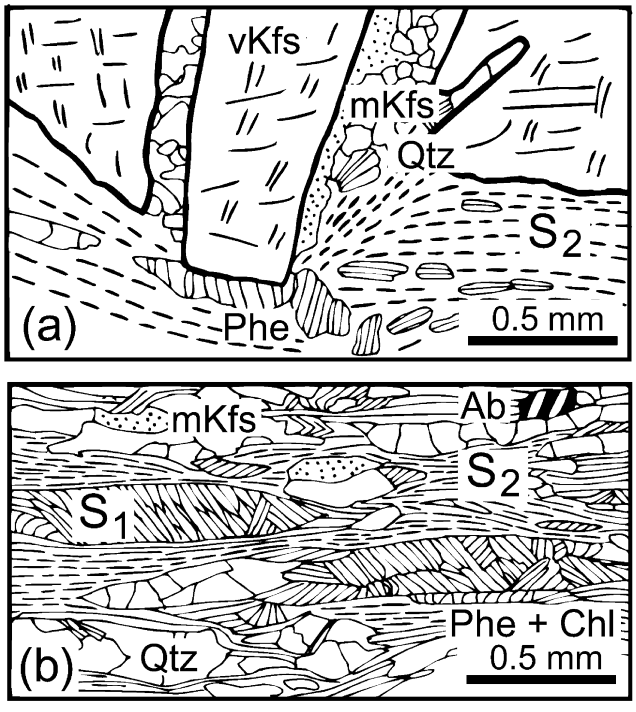

Fig. 2. Microstructures. (a) Metamorphic K-feldspar (mKfs) crystallized in fractures of broken magmatic K-feldspar clasts (vKfs) in a porphyroid. Phengite (Phe) occurs in foliation S2. (b) Microlithons with foliation S1 by phengite and chlorite are surrounded by S2 in a phyllite (sample Kerzo).

Biotite has not been found. The occurrence of chlorite depends on the Fe and Mg bulk rock compositions. The (KFMASH)-equilibrium

3(Fe–Mg)chlorite + 8K-feldspar

$$= 5(\text{Fe–Mg})\text{biotite} + 3\text{muscovite} + 9\text{quartz} + 4H_2O \quad (1)$$

is shifted toward higher temperatures with decreasing bulk *X*FeO (Bucher and Frey, 1994). Accordingly, at given $X\text{FeO}_{WR}$ of about 0.70 and $X\text{FeO}_{Chl}$ of 0.73–0.82, a maximum metamorphic temperature of 430 °C (the formation temperature of biotite at the given bulk rock compositions) has not been exceeded (Fig. 12). Compositions of muscovites signal an exclusive metamorphic origin. They are small phengites, which allowed only one microprobe analysis per grain and show partly green colours. Cationic formulae have been recalculated to 22 oxygens and Fe^{3+} contents were estimated by using the relation $Fe^{2+} = (\text{Si}-3) - (\text{Mg} + \text{Mn} - \text{Ti})$ and $Fe^{3+} = Fe^{tot} - Fe^{2+}$ (Laird and Albee, 1981). Fe–Mg–celadonite contents vary between 30 and 40% except for the samples Penvraz (75–80%) and Kerzo (3.5%). Na contents are low, in the range of 0.01–0.03 for samples Kerdo1 and KerdoT, and the samples from the porphyroids. In the phyllite sample Kerzo, Na is 1.2–0.15 (p.f.u., recalculated to 22 oxygens). The phengite substitutions in samples with K-feldspar vary more (KerdoO, KerdoT) or less (Coter, Kerdo1) and the variations are not dependent on the occurrence of chlorite, albite or the bulk rock composition. Estimates of temperatures are possible from phengite–plagioclase pairs (Green and Usdansky, 1986), from Mg contents (Cipriani et al., 1971), and from Na contents in muscovite (Cipriani et al., 1971). Pressures can be determined in assemblages with phengite, quartz, K-feldspar and phlogopite (Velde, 1967; Massonne and Schreyer, 1987; Massonne, 1995). Restrictions of the Si^{4+} phengite barometer are discussed in Massonne and Schreyer (1987). Absence of tri-octaedral micas in the studied rocks will shift the equilibrium

$$3\text{celadonite} = \text{phlogopite} + 2\text{K-feldspar} + 3\text{quartz} \quad (2)$$

toward higher pressure. The results from rocks without phlogopite then represent minimum pressures. This can be similarly stated when K-feldspar is in the assemblage. Pressures obtained from the calibration by Velde (1967) do not differ significantly (<0.5 kbar) from data obtained by more recent calibrations (Massonne, 1995). Only P–T results from samples with the Fe–Mg phase chlorite have been considered. The Si^{4+} contents in samples Kerdo1 are 6.6–6.7, in KerdoT 6.7–6.8 and in Kerzo around 6.45. This is interpreted to give the pressure variation during the

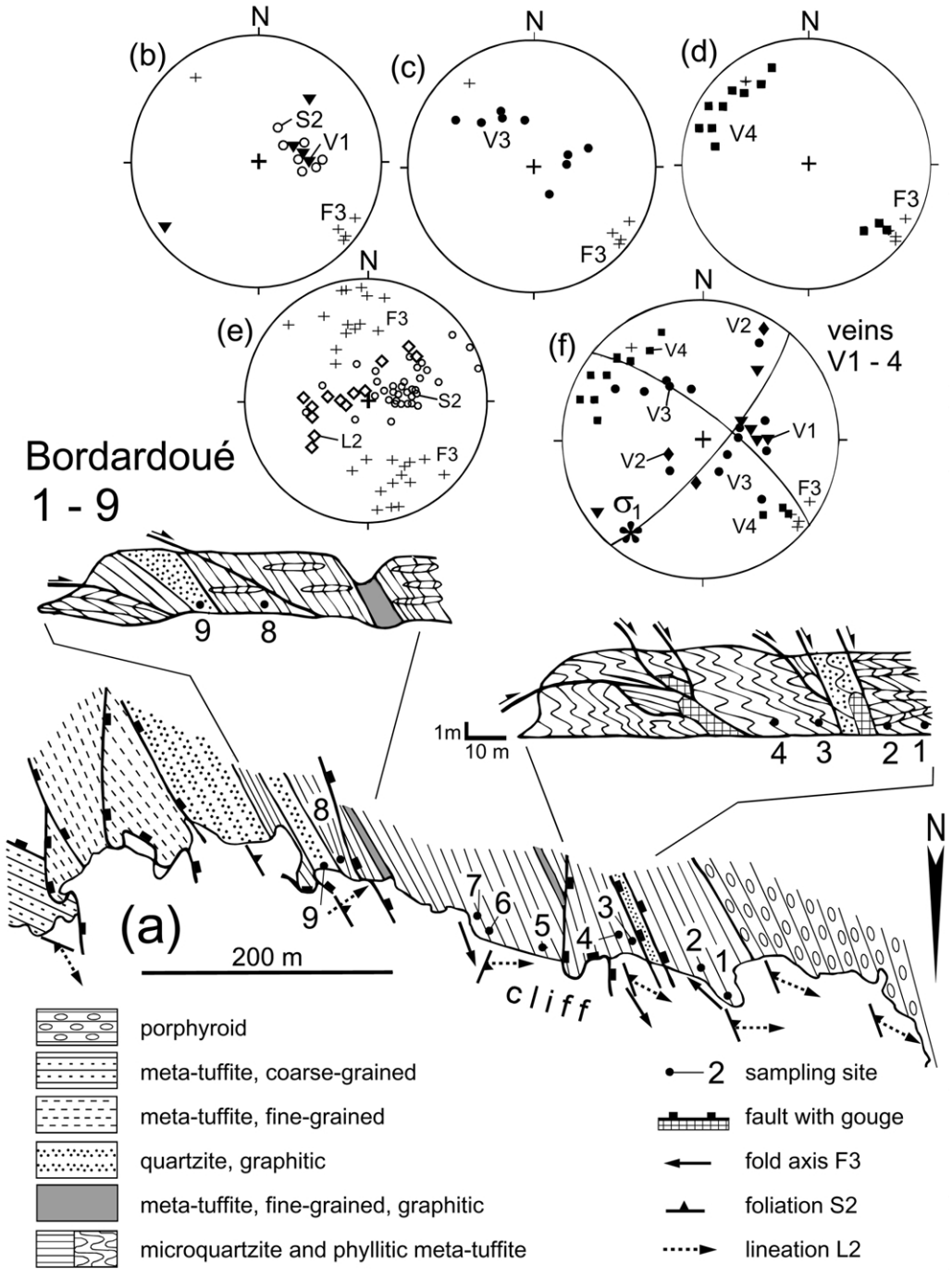

Fig. 3. Structural geology at the plage de Bordardoué (see Fig. 1c). (a) Structural and lithological map with profile sections. Map is turned corresponding to the view of observer on the cliff. Numbers 1–9 are the sample locations (Bor). (b–f) Structural data from Bordardoué in lower hemisphere stereographic projections (Schmidt-net) of linears and plane normals. Orientation data of quartz vein generations V1, V2, V3, V4.

metamorphism (Fig. 12), with sample Kerzo giving the minimum pressure as K-feldspar is lacking. Temperatures estimated from samples Kerdo1 and KerdoT are lower than from Kerzo. However, in detail, calibrations based on the muscovite Mg content (Cipriani et al., 1971) yielded temperatures considerably exceeding the maximum temperatures given by the equilibrium (1) and therefore have been rejected. Temperatures from the muscovite–plagioclase thermometer (Green and Usdansky, 1986) are considerably lower, 200–250 °C for samples Kerdo1/KerdoT and 350 °C for sample Kerzo. As quartz completely recrystallized and shows polygonal and straight grain boundaries in the porphyroid samples, these temperatures appear to be too low and have not been further considered. Temperatures from the calibration based on the Na contents (Cipriani et al., 1971) range from around 400 °C for samples

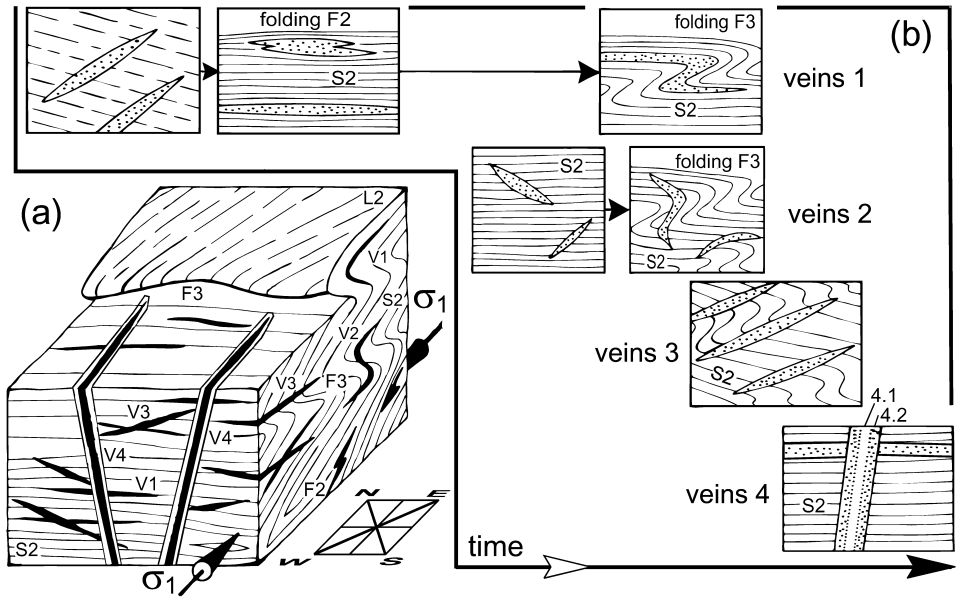

Fig. 4. Structural evolution of quartz veins at Bordardoué. (a) Synthetic block diagram with orientation of quartz veins V1–V4, folds F2, F3, foliation S2, lineation L2 and direction of maximal compressive stress σ_1. (b) Temporal sequence of formation and deformation of quartz vein generations V1, V2, V3, V4.

KerdoT/Kerdo1 to below 450 °C for sample Kerzo, which are next to the upper temperature limit given by equilibrium (1). This appears to give the best approximation of the temperature range at the thermal peak of metamorphism. There is always the same relative difference in temperature estimates from locations Kerdo and Kerzo, whatever thermometer is applied. Microstructures or mineral zonations do not indicate whether these slightly different metamorphic conditions from both locations have been attained along a single clockwise P–T path or signal a more complex thermotectonic history. Whatever, it can be concluded that samples from Kerdo recorded the maximal pressures and sample Kerzo the maximum temperature at lower pressures in the course of the S1–S2 metamorphism (Fig. 12).

4. Structural evolution of quartz veins

Spectacularly folded centimeter- to millimeter-scale interlayering of coarse- and fine-grained meta-tuffites, quartzites, graphitic quartzites and microquartzites occurs at the plage de Bordardoué (Fig. 1c). The structural position of these layered rocks is below a thick porphyroid series, which presumably belongs to the base of the volcano-detrital sequence (Fig. 1d). In general, the foliation of the banded rocks strikes NW–SE, dips to the SW (Fig. 3a and e) and is cut by several normal faults that dip flatly to steeply to the SW (Fig. 3a). Several generations of flat or lenticular veins (veins 1 to veins 4) that consist of pure quartz are observed in the banded rocks. Vein margins and contacts are sharp and straight, the veins are poorly interconnected and there is no wallrock alteration visible. The thickness of the veins ranges between 0.5 and 5 cm; the proportion of the veins in the whole rock volume is less than 10%. Structural evolution and spatial geometrical relations of the veins are illustrated in Figs. 3b–f and 4; the relative temporal succession of vein generations has been directly reconstructed from the cross-cutting relationships.

Quartz veins 1 extend up to 1 m parallel to the lithological layering and foliation S2. It can be speculated that these veins 1 are the fillings of former joints that were rotated parallel to the S1 foliation and the lithological banding

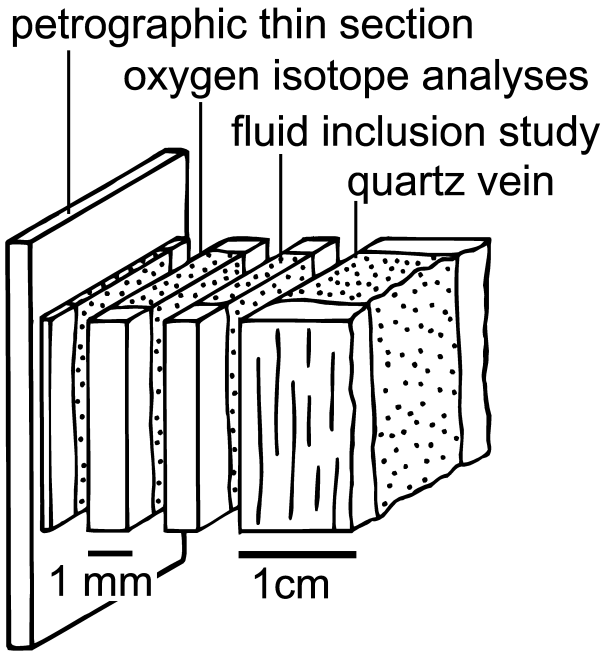

Fig. 5. Sample preparation for petrographic, oxygen isotope and fluid inclusion study of quartz veins.

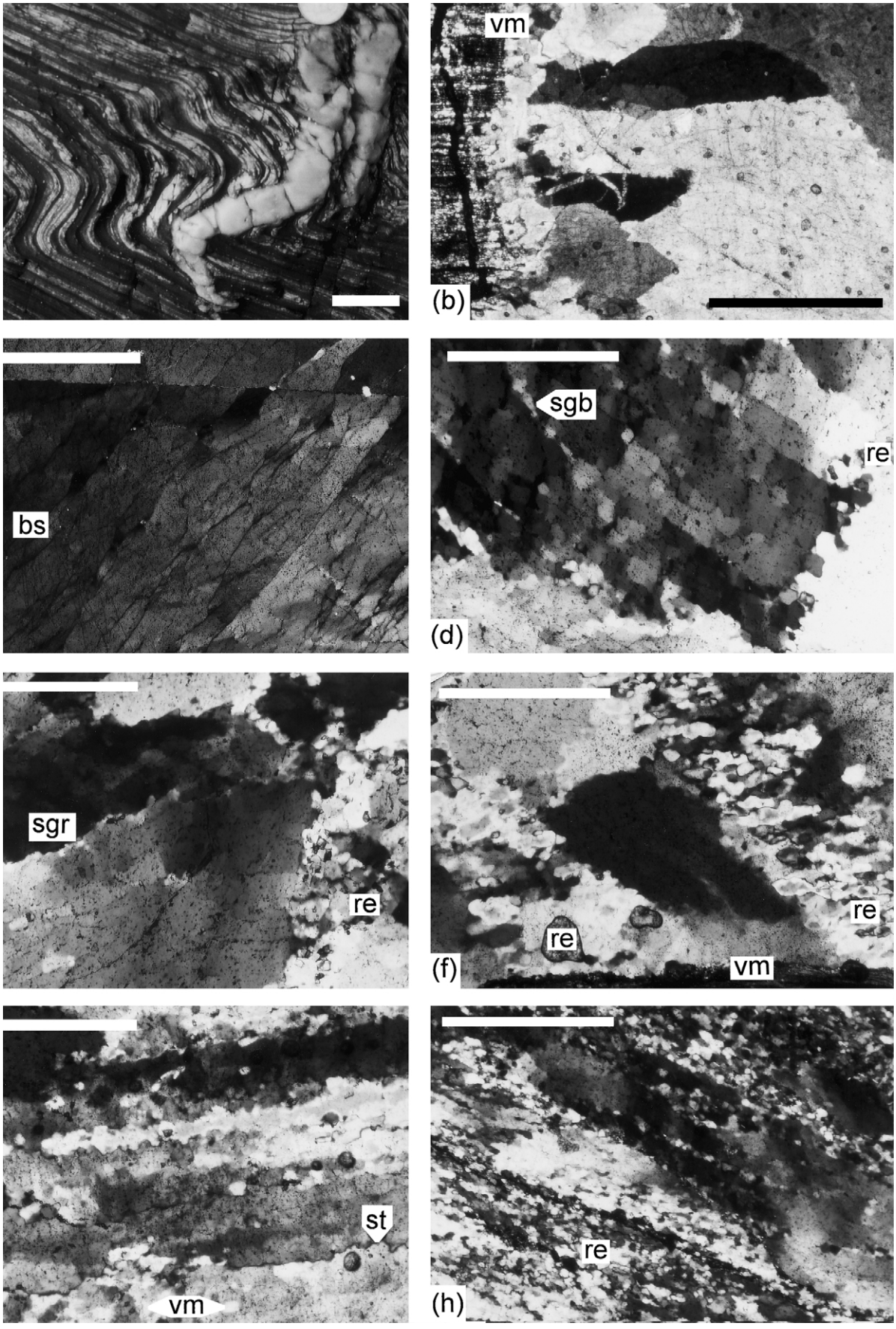
vm
(b)
bs
sgb
re
(d)
sgr
re
re
re
vm
(f)
st
vm
re
(h)

during progressive shearing D1. Foliation S1 and veins 1 have been deformed during D2. Now the veins are oriented parallel to the main foliation S2, which is the axial plane foliation of isoclinal F2 folds (Figs. 3b and 4b). Rod-like structures of the veins 1 are relict hinges of such isoclinal F2 folds. The initially straight quartz veins 1, foliation S2 and the stretching lineation L2 are deformed in F3 folds (Fig. 4b). *Quartz veins 2* are straight and extend several decimeters. They cut S2 at acute angles and were also deformed by folding F3 (Figs. 4b and 6a). Stereographic projections of vein 2 normals are situated along a great circle of which pole fits with F3 fault axes projections (Fig. 3f). The *quartz veins 3* are straight, mostly extend up to 1.5 m, but thin (<0.5 cm) veins with several meters in length occur as well. Veins 3 were not affected by F3 folding. They occur with preferred orientations subparallel to the F3 axial planes and S3. Angles between F3 axial planes and veins 3 do not exceed 20° (Fig. 4a). Thus, veins 3 show different orientations but similar flat dip in single outcrops. When vein 3 orientations from several outcrops are compared, the distribution of the plane normals orientation data is related to a great circle involving the F3 fold axes projections (Figs. 3c and f and 4a). Thus we are dealing here with the conjugate directions of veins of the same generation. Similarly, *quartz veins 4* occur in two conjugate directions. These veins steeply dip to SE and NW and cut across all earlier structures and vein generations and extend from a few decimeters to several meters (Figs. 3d and f and 4b). Sometimes their length exceeds the height of the cliff. Some veins 4 show two successive stages of opening and quartz precipitation. The latest generation of quartz vein filling is next to the wallrock and involves vugs.

Along the cliff at Bordardoué plage, veins 1 are abundant (except at location Bor4) and veins 4 can be observed in many locations (Bor1, Bor3, Bor7, Bor8, Bor9). The veins 3 are obviously related to the sites of intense F3 folding (Bor3, Bor5, Bor7, Bor8), whereas veins 2 are comparably rare (Bor4, Bor6). The critical vertical length, considered as a function of effective normal stress gradient (Secor and Pollard, 1975), apparently strongly increases from mostly subhorizontal veins 1, 2 and 3 to the subvertical veins 4 (Figs. 3f and 4a).

Projections of plane normals of folded veins 1 and 2 are situated along a great circle with a normal matching the F3 axis. Projected plane normals of unfolded veins 2, and of conjugated veins 3 and 4 arrays are geometrically related to another great circle (Fig. 3f). The normal of this great circle should approximate the direction of the principal compressional stress (Figs. 3f and 4a). Thus, at least veins 3 and 4 extend parallel to the maximum stress (Rickard and Rixon, 1983). It is concluded from this geometry that the orientations of the quartz veins 2, 3 and 4 have been controlled by a progressive deformation with a constantly subhorizontal NE–SW oriented principal compressional stress σ_1 (Fig. 4a). The direction of σ_1 is oriented at an acute angle of 15° with the principal plane of displacement (Audren and Gorre, 1995). Extension directions incrementally changed with time as was recorded by the cross-cutting vein generations. As a consequence of their morphology and stress-related geometry, the Bordardoué veins can be interpreted as sites of brittle failure and tension fractures.

5. Petrography and oxygen isotope data of quartz veins

Quartz grains and quartz microstructures in the vein fillings were studied in polished thin sections cut perpendicular to the vein margins (Fig. 5). Veins enclosing fragments of the host rocks are not abundant and were not considered for further study. The quartz grain size in the microquartzite host rocks is <0.01 mm; the quartz grain sizes in the veins range from 0.1 to >1 mm. Internal structures, geometry of grains and morphology of grain boundaries in quartz under polarized light were documented by line drawings and photographs. Petrographical control by cathodoluminescence microscopy (CL) with a hot cathode (Ramseyer et al., 1988; Götze, 1996, 1998) revealed quartz with different cathodoluminescence colors in the veins. The host rock quartz and the original vein quartz veins 1 and 2 have uniform dark brown luminescence. This is interpreted by a formation, or heating of the quartz at temperatures exceeding 300 °C. Small subveins and fissures filled with fine-grained quartz of short-lasting blue and yellow-to-white luminescence colors cut across these veins. These observations, not evident under polarized light, signify that veins 1 and 2 were cracked and refilled. Original quartz fillings in veins 3 and 4 show short-lasting blue and yellow CL and net-like internal optical structures. Sometimes, large vuggy quartz crystals occur at the margins of veins 4. Their cathodoluminescence colors are intense but short-lasting greenish-blue, partly with optical zonations. This indicates a second

Fig. 6. Structures in quartz veins. (a) Vein 2 in banded microquartzites and phyllites, deformed in a monoclinal F3 fold (Bor5), scale bar is 2 cm. (b) Vein margin (vm) of vein 4 with elongate blocky texture of quartz (Bor9-3). (c) Briquette structures (bs) in vein 3 quartz (Bor3-5). (d) Subgrain boundaries (sgb) along former briquette structures and subgrain rotation recrystallization (re) along subgrain and grain boundaries of quartz in deformed vein 1 (Bor3-5). (e) Subgrain boundary formation and subgrain rotation recrystallization (sgr) of quartz in deformed vein 1. Domains with small-grained quartz are labelled (re) as recrystallized (Bor8-5). (f) Domains with small-grained quartz labelled (re) in a deformed vein 1. These domains appear as sealed fractures, are marked by lower values $\delta^{18}O_{SMOW}$ and are connected with the vein margin (vm) (Bor8-21). (g) Strongly deformed vein 1 with quartz grains elongated subparallel to orientation of vein margins (vm). Sugrain rotation recrystallization and sawtooth-like (st) grain-boundaries (Bor9-51). (h) Plastic deformation of quartz and recrystallization by grain boundary migration (re) in vein 2 deformed in F3 folds (Bor4-2). Planar anisotropy is parallel to F3 axial plane. Scale bar in (b)–(h) is 0.5 mm.

stage of opening and re-filling with new quartz along the margins of veins 4. From the short-lasting cathodoluminescence, a formation temperature below 300 °C, and no later heating can be concluded.

Microsamples (1–2 mg, 1 mm in diameter) have been broken from thin plates matching the petrographical thin sections (Fig. 5). Each microsample consists of 1–3 pieces of quartz; the study is based on 100 analyzed microsamples. They have been extracted under a BrF_5 atmosphere with a 20 W CO_2 laser and the liberated O_2 has been directly analyzed in a modified Finnigan MAT 251 mass spectrometer, as described in detail by Sharp (1992, 1995). Microsamples from the same plate (thin section) have been analyzed in different runs. The oxygen isotope data is reported in permil (‰) $\delta^{18}O_{SMOW}$ without corrections or further modifications. Overall precision of the analyses, compared with standard quartz Lausanne 1 (18.15‰) is 0.2‰.

Quartz grains in veins 3 and 4 show only slight or no deformation and allowed the recognition of a growth direction. Criteria for syn-, anti- and ataxial quartz growth in veins were reported by Ramsay and Huber (1983), Passchier and Trouw (1996) and Bons (2000). Growth mechanisms were described by Cox and Etheridge (1983) and modelled by Bons and Jessell (1999). Signs of antitaxial growth, from the center (c) toward the margin (m), as median lines of wallrock fragments in the centers of the veins or aligned fluid inclusions parallel to the vein margins are not obvious in the samples. In all studied cases, grain sizes of quartz are small along the vein margins. Sizes of quartz grains with the long axis perpendicular to the vein margins increase toward the center of the veins (Figs. 6b and 7a and c). This is considered as the elongate blocky texture (Fisher and Brantley, 1992), which gives evidence of crystallographically (face) controlled growth competition between grains (Cox and Etheridge, 1983) and which is typical of syntaxial (from the margin to the center) vein quartz growth. The quartz grains show the characteristic internal briquette-like structure (Fig. 6c) as a sign of primary crystallization and saw-tooth or serrated as well as straight grain boundaries are observed. Series of continuous inclusion bands parallel to the vein margins and reported as diagnostic by Ramsay (1980) and Fisher and Brantley (1992) are not evident in the veins. When not disturbed by later opening and re-sealing, the $\delta^{18}O$ of quartz decreases by about 1–2‰ toward the center of the veins (Figs. 7a and c, 8a, c and d and 10c). A clear tendency of lower $\delta^{18}O$ in younger veins is characteristic in cross-cutting vein generations (Figs. 7c and 10a–c). There, quartz of the younger veins displays syntaxial crystallization with the same crystallographic orientation as quartz belonging to the older vein.

Cross-cutting of vein 1 by a vein 4 led to a decreasing average quartz grain size in the older vein toward the contact. This is accompanied by decreasing $\delta^{18}O$ (Fig. 7c). The small quartz grains in the contact zone are therefore

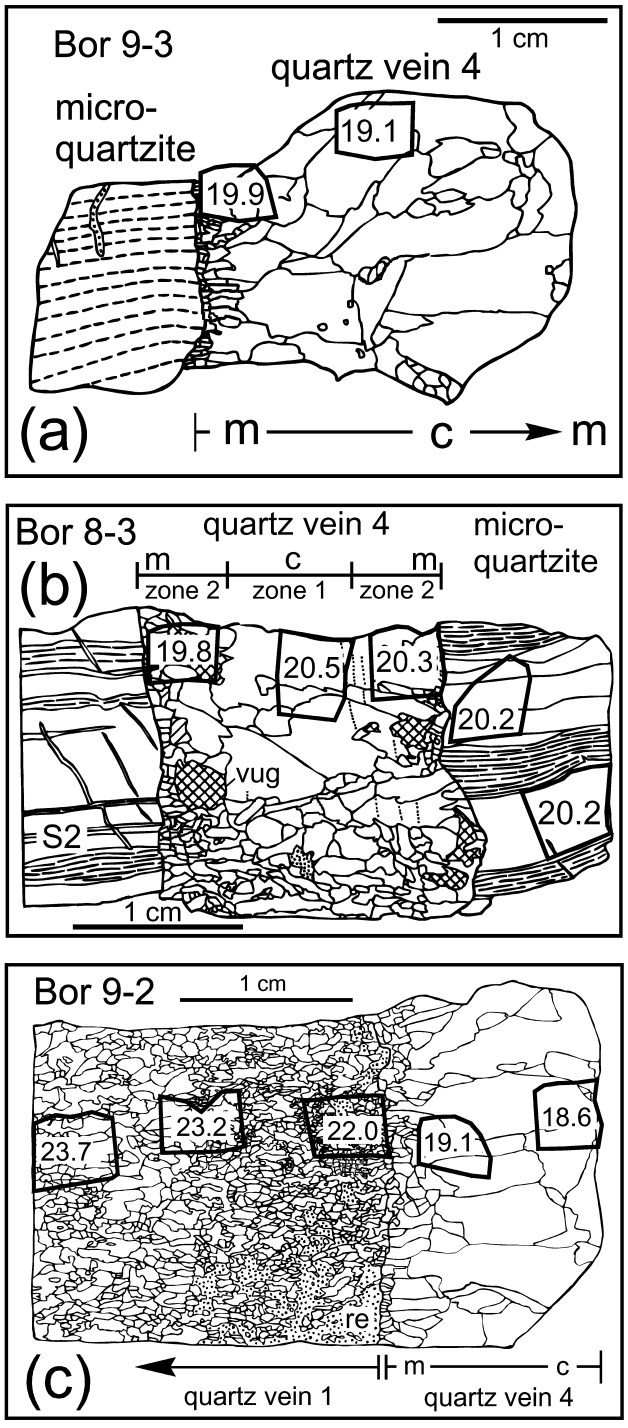

Fig. 7. Quartz grain shapes and microstructures (drawn from thin sections) in single quartz veins and in cross-cutting veins of different generations. Numbers are oxygen isotope data (in ‰ $\delta^{18}O_{SMOW}$) from quartz and microquartzite; lines mark the size of the microsamples. Margin (m) and center (c) of the veins. (a) Vein with elongate blocky texture of small quartz grains at the margin and large grains in the center, indicating syntaxial growth (compare with Fig. 6b). (b) Vein 4 with later opening and precipitation in a zone 2 with vugs (cross-hatched) along the margin. (c) Vein 4 cuts across vein 1. Domains with small-grained quartz, which apparently invaded from vein 4 (re) are dotted.

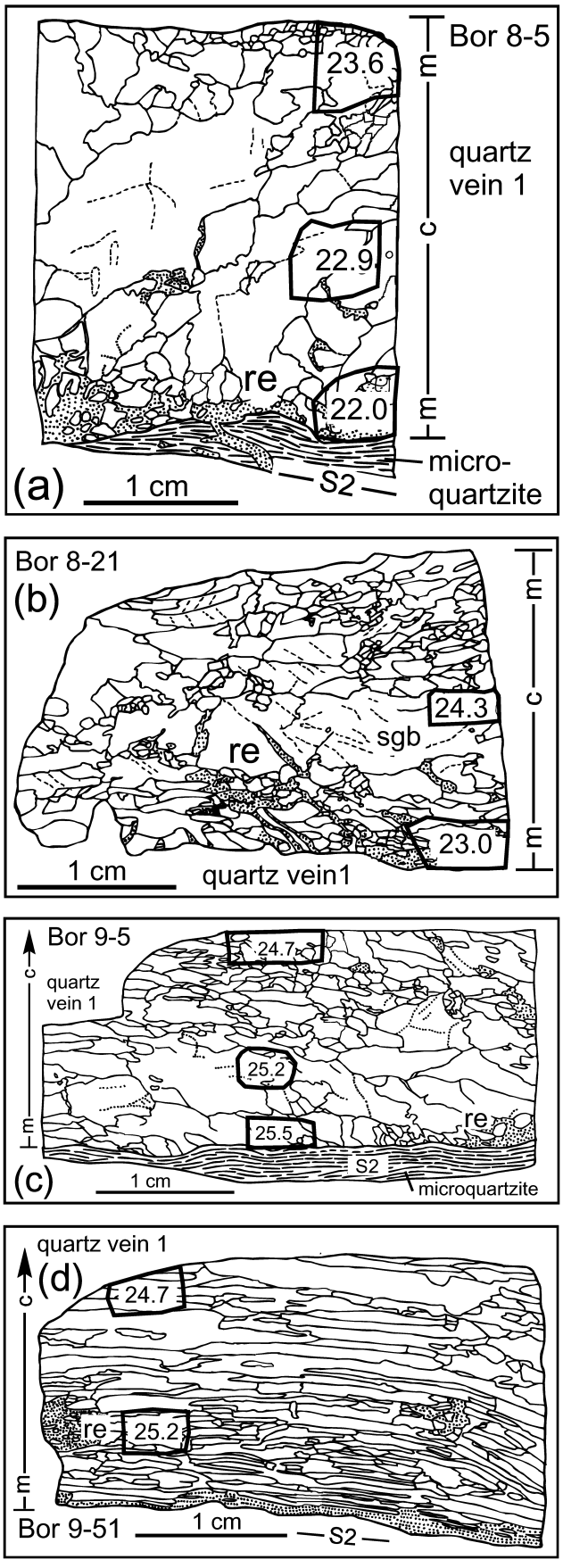

interpreted not to have recrystallized along the margins of larger old grains, but to have precipitated from silica infiltrated during the formation of the younger vein. The increasing proportion of such small new grains with low values $\delta^{18}O$ can explain the decreasing $\delta^{18}O$ in the old vein toward the contact with the younger vein. Some of the veins 4 show a zonation with vugs along the margin,

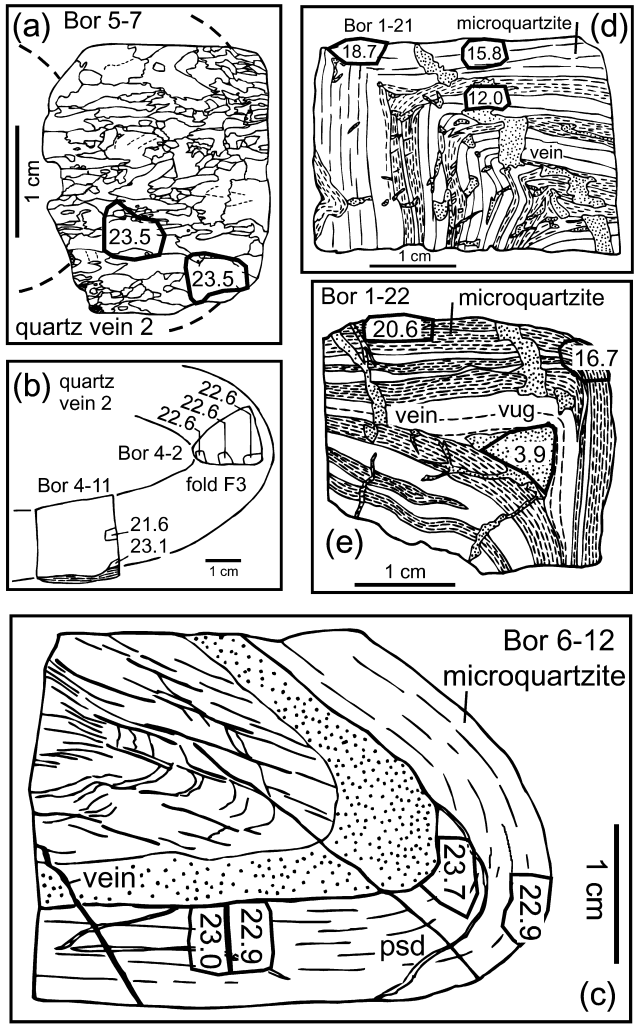

Fig. 9. (a) Quartz grain shapes and microstructures (drawn from thin sections) in folded (F3) quartz vein 2. (b) Position of samples and quartz oxygen isotope data in folded (F3) quartz vein 2. (c–e) Microstructures in folded (F3) microquartzites. A pressure solution domain (psd) appears in a fold hinge. Numbers are oxygen isotope data (in ‰ $\delta^{18}O_{SMOW}$) from quartz; lines indicate sizes of microsamples.

Fig. 8. Quartz grain shapes and microstructures (drawn from thin sections) in quartz veins 1. The figures of the veins are arranged with increasing strain (from (a) to (d)). Numbers are oxygen isotope data (in ‰ $\delta^{18}O_{SMOW}$) from quartz; lines indicate sizes of the microsamples. Margin (m) and center (c) of the veins. Domains with small-grained quartz, labelled as recrystallized (re) are dotted. Domains of small-grained quartz in (a) and (b) have lower values of $\delta^{18}O$ and are connected with the vein margins and wallrock.

underlined by quartz with short-lasting greenish-blue CL. These veins underwent a second stage of opening at the margins and a partial re-filling with quartz lower in $\delta^{18}O$ (Fig. 7b).

Criteria of growth direction are difficult to assess in quartz veins 1, as these have been affected at least by deformation D2. Microstructures in a range of increasing strain are compared in Fig. 8. With increasing strain, long axes of quartz grains have acute angles or are subparallel to the vein margins (Fig. 8a). However, in some cases the grain size distribution with smaller grains along the margin, reminiscent of syntaxial crystallization, can be observed in lower strained veins 1 (Fig. 8a and c). A tendency toward lower $\delta^{18}O$ in the center of veins, as from veins 2, 3 and 4, is observed (Fig. 8a, c and d). Quartz grains show internal subgrain boundaries that follow the former briquette structures (Fig. 6d). The grain boundaries have a saw-tooth or serrated morphology (Fig. 6d–g). A subgrain rotation recrystallization occurs along microfaults, which developed along the subgrain and grain boundaries of the large quartz crystals (Fig. 6d, e and g). These domains with small recrystallized quartz grains should be distinguished from domains and fissures with similar small grain sizes and partly extending to the wallrocks (Fig. 6f). The latter domains are characterized by lower values $\delta^{18}O$ compared with the original vein quartz (Fig. 8a and b).

Quartz in the hinges of veins 2 deformed in F3 folds show plastic deformation and recrystallization by grain boundary migration (Fig. 6h). This indicates that temperatures should have still exceeded 300 °C during folding D3 (e.g. Passchier and Trouw, 1996; Stöckhert et al., 1999). Although an increasing flattening strain toward the inner part of the fold hinge is observed, the $\delta^{18}O$ of quartz does not vary across the fold hinge. The values in the fold hinge are intermediate between the values analyzed in the zoned vein with subgrain rotation recrystallization in the flank of the fold (Fig. 9a and b).

Folded (F3) microquartzites have been analyzed as well, however, the microsampling is complicated by small quartz veins that fill the extensional domains of the fold hinges (Fig. 9d and e). These syn/post-F3 veins intruded during brittle deformation at a late stage or after folding, and are partly filled with vuggy quartz. They have very low $\delta^{18}O$ values when compared with the microquartzites. These late veins cut across pressure solution domains, which compensate compression in the fold hinges (Fig. 9e). Values of $\delta^{18}O$ in microquartzite fold hinges and fold limbs vary over about 2‰. This presumably is caused by unintentional sampling of the late vein fillings with low $\delta^{18}O$ (Fig 9d and e). In a folded microquartzite bearing only very thin late veins of which contribution to the whole-rock value $\delta^{18}O$ should not be significant (Fig. 9c), similar $\delta^{18}O$ are observed in flanks of the folds and the extensional domain of the fold hinge (22.9–23.0‰). The compressional domain of the fold hinge is connected with a pressure solution domain and gives a significantly higher $\delta^{18}O$ of 23.7‰ (Fig. 9c).

To sum up, in profiles across single veins that have not been affected by later recrystallization or new invasion of quartz, and on the condition of syntaxial growth, a decrease of $\delta^{18}O$ of about 1–2‰ during vein crystallization can be derived (Fig. 10c). When the data from the vein generations is compared, especially from cross-cutting veins of different generations, the $\delta^{18}O$ show a general decrease from veins 1 to veins 4 of about 3‰ (Fig. 11a and b). Early veins 1 have been opened, cracked and refilled by quartz with lower $\delta^{18}O$. This general tendency toward lower $\delta^{18}O$ with time is continued in folded microquartzites with late veins of very low values of $\delta^{18}O$.

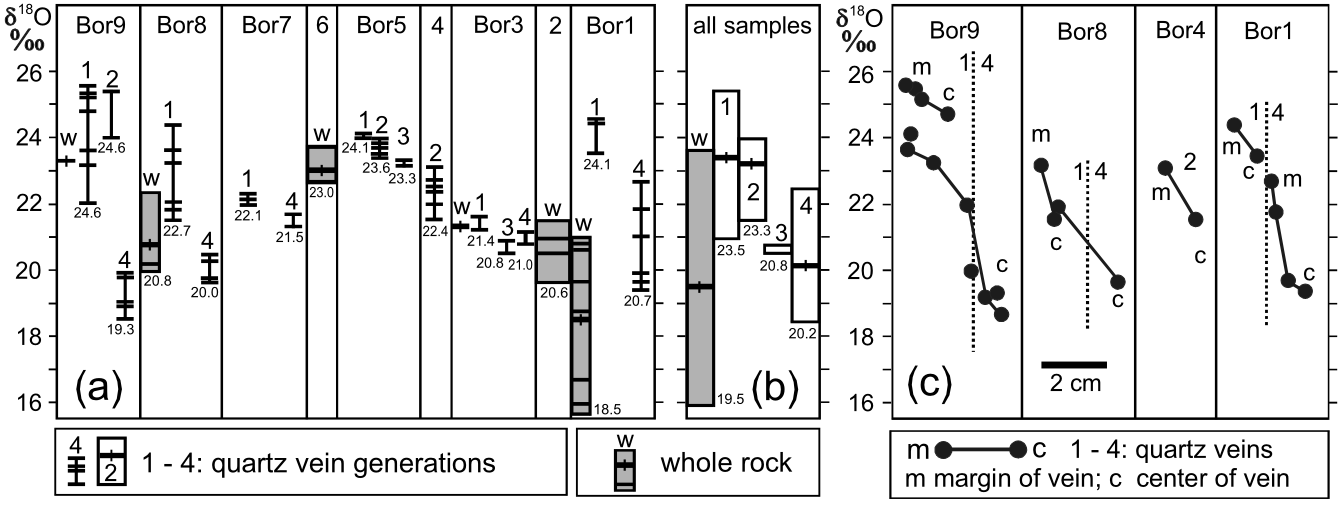

Fig. 10. Oxygen isotope data in quartz vein generations (1, 2, 3, 4) and in microquartzite whole rock (w) from locations Bordardoué 1 to 9. (a) Data compiled from each location. Horizontal bars mark analyses from single vein generations; numbers below vein generation and whole rock columns are the statistical means. (b) Data compiled for whole rocks and each vein generation. (c) Data in profiles of veins and cross-cutting vein generations. m = margin, c = center of veins.

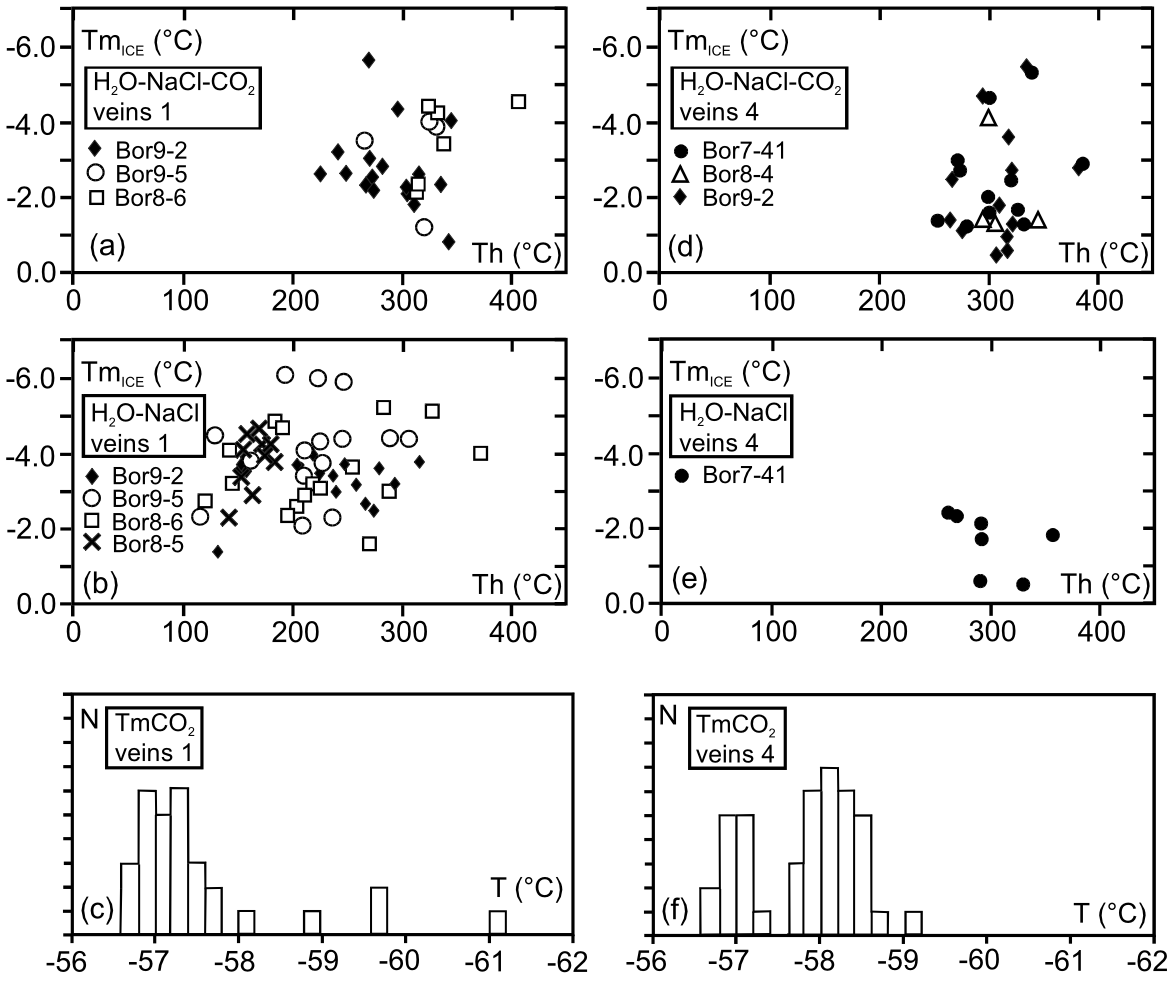

Fig. 11. Fluid inclusion microthermometry data from quartz veins 1 and 4. (a, b, d, e) Homogenization temperatures T_h (to the liquid) versus ice melting temperatures $T_{m\ ICE}$. (c, f) Distribution of CO_2 homogenization temperatures to the liquid $T_{m\ CO_2}$. Bimodal distribution in veins 4 signalizes traces of CH_4.

6. Fluid inclusion study

As quartz microstructures and oxygen isotope values in veins 1 and 4 show marked differences, the fluid inclusion study concentrates on these vein generations. The question arises, whether fluid compositions and fluid entrapment conditions may have changed during the successive vein formation. Gravimetric estimates (quartz veins have 2.60–2.58 g/cm^3, trigonal pure quartz has 2.65 g/cm^3) led to a maximum 3–7% proportion of fluid inclusions (1.0 g/cm^3) within the veins. Microthermometric measurements on 240 fluid inclusions (FI) have been performed on seven doubly-polished quartz vein samples from Bordardoué (Fig. 5) with an USGS Type REYNOLDS Fluid Inc. heating–cooling system (Goldstein and Reynolds, 1994). The cycling technique (Roedder, 1984; Goldstein and Reynolds, 1994) was used. All samples are dominated by domains with milky quartz, which is not suitable for FI study. Microscopical control of 3–5 mm^2 sized chips broken from double-side polished thin sections revealed some domains within the quartz briquette structures which bear small (0.015–0.02 mm) H_2O–NaCl and H_2O–CO_2–NaCl inclusions. The FI morphologies are hexagonal with negative crystal shapes, flat, long prismatic, short prismatic and partly with concave boundaries, as is considered typical of primary inclusions. As no systematic correlation of morphology or geometrical arrangement and fluid compositions is observed, the FI have been assigned to a single generation. The veins display polygonal to linear distribution of FI, partly coincident with the briquette structures (Fig. 6b and d). However, a correlation of deformation, geometrical arrangement and homogenization temperatures of FI as in the studies of Kerrich (1986), Drury and Urai (1990), O'Hara and Haak (1992) has not been established here. There is a presence of numerous secondary FI aligned along microfractures in veins 1. The small size (<0.005 mm) of these inclusions allowed no analysis. Recrystallized small quartz grains in veins 1 bear no FI.

Homogenization was, in all cases, to the liquid phase. Temperatures of homogenization to the liquid (T_h) in H_2O–CO_2–NaCl inclusions in veins 1 range between 220 and 350 °C. $T_{m\ ICE}$ (melting of the solid) of these inclusions are between −2.0 and −5.0 °C, with a statistical accumulation around −3 °C (Fig. 11a). A similar range of

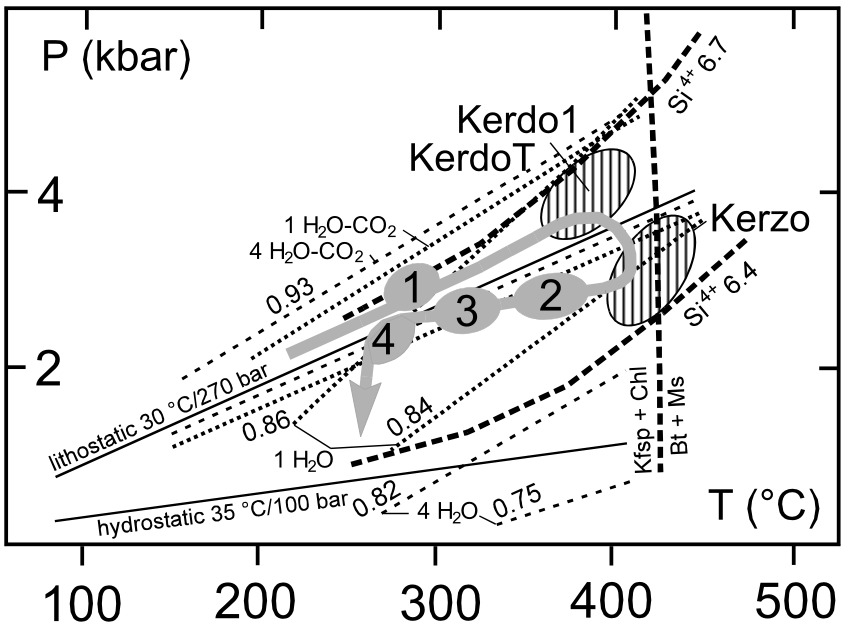

Fig. 12. Thermobarometry of Belle-Ile porphyroids and phyllites, based on phengite Si^{4+} (Velde, 1967) and Na contents (Cipriani et al., 1971) (hatched domains) and mineral equilibria (thick broken lines), compared with isochores calculated for veins 1 and 4 fluid inclusion compositions (broken lines, numbers are g/cm^3). Arrow 1–2–3–4 indicates presumed formation conditions of quartz vein generations 1, 2, 3, 4.

T_h (250–380 °C) is found from H_2O–CO_2–NaCl inclusions in veins 4. $T_{m\,ICE}$ of these inclusions ranges from −0.5 to −5.0 °C, with a statistical mean and accumulation around −1.5 °C (Fig. 11d).

In contrast, the H_2O–NaCl inclusions in veins 1 display a broad range of T_h between 120 and 350 °C with statistical accumulations around 150, 230 and 280 °C (Fig. 11b). One vein 1 (sample 8-5) has only H_2O–NaCl inclusions with T_h around 180 °C and $T_{m\,ICE}$ of −4.0 °C. The range of T_h of H_2O–NaCl inclusions in veins 4 is 250–350 °C and matches the data from the H_2O–CO_2–NaCl inclusions.

Depression of temperatures $T_{m\,CO_2}$ of < -56.6 °C is suggested to be the result of contamination of CO_2 by traces of CH_4 or H_2S in these inclusions. The $T_{m\,CO_2}$ from veins 1 show a unimodal distribution around −57.0 °C, which gives no hint of a significant contribution of CH_4 to the fluid (Fig. 11c). A bimodal distribution around −57.0 and −58.2 °C is observed for veins 4 and may signal a proportion of CH_4 in the fluid (Fig. 11f). Temperatures $T_{m\,CLA}$ of clathrate melting exceeding 10 °C are frequently observed in veins 4 and never occur in veins 1. This is also strongly supportive of the presence of CH_4 in FI of veins 4 (Diamond, 1994).

Salinities, densities and isochores of H_2O–NaCl and H_2O–CO_2–NaCl inclusions have been calculated using the equations of state proposed by Zhang and Frantz (1987) and Brown and Lamb (1986, 1989) in FLINCOR (Brown, 1989, 1998). Within a wide range, the salinities in both H_2O–NaCl and H_2O–CO_2–NaCl inclusions are higher in veins 1 (4–8% NaCl) than in veins 4 (1–4% NaCl). This is indicated by the lower $T_{m\,ICE}$ in veins 1 compared with veins 4. Estimates of X_{CO_2} in FI yielded a range of 0.05–0.25 for veins 1 and 4, but the statistical distribution of analyses indicates a lower X_{CO_2} in veins 4, which coincides with the indications for CH_4. To sum up, the data from fluid inclusions indicate a change of the fluid composition in the time span from precipitation of veins 1 to veins 4. CO_2 is present in FI of both vein generations, but X_{CO_2} decreases in veins 4 due to the presence of CH_4. This is accompanied by a decrease of the salinity.

Estimates of gaseous CO_2 in fluid inclusions are afflicted with large uncertainty of about ±5% (Roedder, 1984), but correspond to a negligible ±0.02 g/cm^3 in isochore calculations. The isochores in Fig. 12 have been calculated from inclusions that represent the statistical accumulations of the analyzed T_h and $T_{m\,ICE}$. Densities of H_2O–CO_2–NaCl inclusions in veins 4 are similar to those in veins 1 (0.93–0.86 g/cm^3). These high-density H_2O–CO_2–NaCl inclusions apparently represent the original entrapment conditions of the fracturing event along a lithostatic gradient of about 30 °C/270 bar (Fig. 12).

H_2O–NaCl inclusions in veins 1 have partly lower densities of 0.90–0.84 g/cm^3 and higher T_h when compared with the CO_2-bearing inclusions (Figs. 11b and 12). Post-entrapment change of densities in fluid inclusions can occur when the cooling–decompression path of the sample shows a significant deviation from the original isochore. Corresponding experiments with isothermal decompression (Vityk and Bodnar, 1995) led to an increase of T_h and decrease of densities in inclusions. It has to be kept in mind that veins 1 underwent deformation. As has been experimentally investigated by Sterner and Bodnar (1989) or Bakker and Jansen (1990), post-entrapment inelastic volume change, diffusion, inclusion leakage and stretching

occur in quartz during deformation. FI density decrease and T_h increase could be driven by these processes when the P–T evolution deviates from original isochores. T_h in such changed FI approach the maximum temperature conditions during the re-equilibration. Preferred re-equilibration of H_2O–NaCl inclusions compared with H_2O–CO_2–NaCl inclusions has been reported by Hall and Wheeler (1992).

In contrast, H_2O–NaCl inclusions in veins 4 exclusively show high T_h and low densities of 0.82–0.75 g/cm^3, along and below hydrostatic conditions (Figs. 11e and 12). As H_2O–CO_2–NaCl inclusions in veins 4 show high densities and post-entrapment deformation in veins 4 is not significant, the leakage model appears unlikely. An alternative explanation has been described by Henderson and McCaig (1996): pressure could change during quartz precipitation in a single vein. Lithostatic conditions will be built up and maintained during long periods between distinct seismic events. Relaxation to hydrostatic values then is possible during and after the short-lasting earthquake event. Fast changes to hydrostatic conditions would be in accordance with the observation of vugs in the second opening stage, the orientation and the large subvertical extension of the analysed vein 4 at Bor7.

7. Discussion of quartz–H_2O–CO_2 interactions

Vein quartz is precipitated from silicious solutions (e.g. Fournier, 1985). Fisher and Brantley (1992) discussed models of quartz overgrowth and vein formation in the light of petrographic observations. They favored diffusive flux from adjacent matrix rocks as a silica transport mechanism after each dilatational event to explain the textural features of crack-seal veins. Periodically repeated incremental dilatation and sealing, induced and triggered by seismic events (Sibson et al., 1975) can accrete to complete centimeter-thick crack-seal veins (Ramsay, 1980). At Bordardoué the corresponding petrographically diagnostic regular inclusion lines parallel to the vein margin are lacking or scarcely recognizable; one may speculate about a more continuous opening and sealing process.

Values of $\delta^{18}O$ in veins reflect the isotopic character of the fluid and temperature-dependent fractionation. The source of the silica in these solutions is the dissolution of quartz in rocks nearby or at a larger distance. These rocks may control the isotopic characteristics of the fluid. Meteoric and metamorphic or magmatic as well as locally hosted water are potential sources of the fluid. Compared with data from other metamorphic terrains and rock types (Hoefs, 1997), the whole-rock values of $\delta^{18}O$ from the Bordardoué microquartzites are high and reach nearly 24‰ with a statistical mean of 19.5‰ from all analyses (Fig. 10a and b). They considerably exceed values of 15‰ reported from acid volcanic rocks (Hoefs, 1997), even when the effects of metamorphic devolatilization with a potential increase of +1‰ (Valley, 1986) are considered. These high maximum values of $\delta^{18}O$ of the microquartzites cannot be caused by an interaction and isotopic exchange of the rocks with a pervasive external fluid. Fluids of metamorphic origin are expected to have comparably lower values of $\delta^{18}O$. Fluids derived from carbonate rocks may be rich in ^{18}O; but marbles do not occur in the lithological pile in Belle-Ile. Thus, the observed high $\delta^{18}O$ in the host rocks should represent their original isotopic signature. Biogenic cherts with potentially high $\delta^{18}O$ (Hoefs, 1997) are the probable protoliths of the microquartzites, and with the interlayering graphitic rocks, they are peculiar in the volcano-detrital sequence of Belle-Ile. When these ^{18}O-rich host rocks are considered as the source of the vein quartz and as a buffer of the dissolving fluid, one could expect veins with comparably high values of $\delta^{18}O$ in quartz.

Values of $\delta^{18}O$ of veins 1 partly even exceed the high whole-rock values in the host rocks (Fig. 10a and b). This is also true when the statistical means are compared. A comparable observation has been reported by Slater et al. (1994) from very low-grade rocks and veins. This is in marked contrast to what is commonly found in metamorphic rocks, where veins have similar (Hoernes and Hoffer, 1985; Yardley and Bottrell, 1992) or lower (Kirschner et al., 1993, 1995) values of $\delta^{18}O$ as host rock matrix quartz.

The observation of higher $\delta^{18}O$ in veins as in the host rocks is difficult to explain. Fractionation equations for the system H_2O–SiO_2 are well established (Friedman and O'Neil, 1977; Matsuhisa et al., 1979; O'Neil, 1986). Accordingly, when the version of the fractionation equation determined by Matsuhisa et al. (1979) is used ($\delta^{18}O_{QUARTZ} - \delta^{18}OH_2O = 10^3 \ln\alpha Quartz - H_2O = -3.31 + 3.34(10^6/T^2)$), the fluid should have lower values $\delta^{18}O$ when in equilibrium with host rock quartz. At constant temperature, quartz precipitated from this siliceous fluid will have values of $\delta^{18}O$ similar to the host rocks. Quartz will be slightly enriched in ^{18}O when precipitated from fluid flowing down temperature (Fourcade et al., 1989; Dipple and Ferry, 1992b). The observed high values of $\delta^{18}O$ in the vein quartz could indicate the contribution of a fluid with high values of $\delta^{18}O$. At Bordardoué and Belle-Ile, marbles as a potential source of fluids with high $\delta^{18}O$ (Hoefs, 1997) are completely lacking. Phyllosilicates have lower values of $\delta^{18}O$ as quartz when in equilibrium at metamorphic conditions (Friedman and O'Neil, 1977; Matsuhisa et al., 1979). Detrital mica, discussed as a possible source of ^{18}O by Slater et al. (1994) is not preserved in the rocks in Belle-Ile. As stated above, one can even exclude a fluid from an external source, as such metamorphic fluids usually have considerably lower $\delta^{18}O$ (Hoefs, 1997). When external sources of ^{18}O fail, a local enrichment process of $\delta^{18}O$ in the fluid should be considered.

At Bordardoué, fluid inclusions give evidence of the presence of CO_2 during vein formation. From the

abundant graphitic layers, the CO_2 could have generated by O_2-bearing fluids by the reaction

$$C_{GRAPHITE} + O_{2FLUID} = CO_{2FLUID}$$

According to Friedman and O'Neil (1977), in the system of CO_2–H_2O the $10^3 \ln\alpha CO_2$–H_2O at temperatures of 250–350 °C is around 15–11‰. When in equilibrium with a whole-rock quartz of 24‰ at 250 °C, the H_2O would have a $\delta^{18}O$ of 15‰ ($\delta^{18}O_{QUARTZ} - \delta^{18}O_{H_2O} = 10^3 \ln\alpha Quartz - H_2O = -3.31 + 3.34(10^6/T^2)$; Matsuhisa et al., 1979). The CO_2 in equilibrium with such water then would have a value of $\delta^{18}O$ of 30‰. This CO_2 is therefore a potential source of ^{18}O. When quartz is precipitated from silicious fluid in the presence of such dissolved CO_2, it could be as well enriched in ^{18}O.

Several aspects can be discussed to explain the decreasing $\delta^{18}O$ during the crystallization of a single vein. Kirschner et al. (1993) found variable enclave thickness and spacings of homogeneous high $\delta^{18}O$ host rock and low $\delta^{18}O$ vein quartz to be responsible for the isotopic zonation in crack-seal veins. Petrographic observations in the Bordardoué quartz veins provided no arguments for such host rock enclaves. Precipitation or crystallization of quartz from an isotopically homogeneous fluid source during decreasing temperature would lead to increasing $\delta^{18}O$ in quartz toward the younger parts of a vein. Otherwise, a decrease in $\delta^{18}O$ of 2‰ from the vein margin toward the center as at Bordardoué would then require an increase of temperature of about 60 °C during the crystallization of a single vein generation. However, there are no other arguments (e.g. from the FI study) that support such a temperature increase during the formation of a single vein. Another point of argumentation is given by the possibility of a changing isotope composition of the fluid from which the silica precipitates. When a mixed fluid $H_2O + CO_2$ is present, as has been outlined before, a successive removal of CO_2 as source for ^{18}O from the fluid would cause decreasing $\delta^{18}O$ in quartz during precipitation. Another explanation could be an increasing contribution of isotopically light meteoric water in the fluid during quartz precipitation. Whatever, the isotope variations across single veins signify that the fluid reservoir during the crystallization period of a single vein generation was not infinite but underwent changes with time. Thus, precipitation of the vein quartz can be considered as a comparably long-lasting process, giving enough time to record changing fluid composition or temperatures, whatever. The isotopic changes indicate, moreover, that we are dealing here with a limited and localized fluid system, which contrasts giant crustal scale (>10 km) fluid systems with isotopically homogeneous external fluids, as described by Oliver et al. (1993).

Other constraints on the dimension of the fluid system arise from decreasing NaCl contents in the fluids and the decreasing $\delta^{18}O$ in quartz in younger generations of veins. These observations point to changes in the fluid compositions. The FI study provided data that favor the presence of CH_4 in the fluid from which vein quartz 4 has been precipitated. This could also decrease the $\delta^{18}O$ of the precipitated vein quartz 4. A considerable metamorphic cooling, and thus a decreasing $\delta^{18}O$ of the fluid in equilibrium during the host rock dissolution, in accordance with the quartz–H_2O fractionation equation of Matsuhisa et al. (1979), appears as a possible mechanism for successively lower $\delta^{18}O$ in younger veins. However, such a metamorphic cooling is not substantiated by the fluid inclusion data. An increasing contribution of a reservoir with low $\delta^{18}O$ to the fluid, as meteoric water, could attribute for decreasing $\delta^{18}O$ in the fluid and thus for decreasing $\delta^{18}O$ in the vein quartz generations, which crystallized from the fluid. The slightly decreasing salinities in the fluid inclusions from veins 1 to veins 4 substantiate such an explanation. Especially vuggy quartz with $\delta^{18}O < 10‰$ in folded microquartzites should have been precipitated under the presence of isotopically light meteoric water.

Quartz vein generations 1 and 2 as well as microquartzitic host rocks were sheared and folded. This led to pressure solution domains in microquartzites. Pressure solution domains show an increase of $\delta^{18}O$. Quartz recrystallized in the veins. Domains with quartz subgrain rotation recrystallization along planar microfractures and former briquette structures conserve initial isotopic compositions. Subgrain rotation recrystallization involves the mechanical tilting of the crystal lattice. This process should keep atoms within a given domain. In contrast, grain boundary migration recrystallization is characterized by an incremental move of material passing through crystal domains. This appears as a possible mechanism to explain the observed isotopic homogenization in the deformed veins 2.

However, in veins 1, larger domains of up to 1 mm^2 (in thin sections) with quartz of small grain size, labeled as recrystallized, are characterized by lower $\delta^{18}O$. These domains are often situated close to the vein margins and/or are connected with small veins extending into the wallrock. CL petrography indicates penetration of veins 1 by small veins of different quartz. In the course of a deformation, the veins 1 will be fractured, especially along the margins. On one hand this would have opened pathways for fluids and the invasion of new quartz from the wallrocks into the pre-existent vein. On the other hand, quartz in the pre-existent vein could have been mobilized and precipitated in these fractures. The fractures can also be expected to be the preferred sites of recrystallization induced by the deformation (Bons and Jessell, 1999; Van Daalen et al., 1999). Lower values of $\delta^{18}O$ in such domains with the small quartz grains indicate the presence of 'new' quartz. It is not possible to distinguish whether this quartz comes from internal dissolution and re-precipitation within the pre-existing vein or invaded from the wallrocks with their general tendency to lower values of $\delta^{18}O$ in younger vein generations. Observations and isotope composition

profiles in cross-cutting vein generations (Fig. 7c) favor the invasion of quartz into a pre-existent vein.

8. Conclusions

At Bordardoué, the quartz vein generations 1–4 successively crystallized in fine-banded quartz-rich host rocks at conditions between 300 and 400 °C during a multistage Variscan deformation. Inclusion lines parallel to the vein margins are not always obvious, but elongated blocky textures provide the argument for the crack-seal mechanism of vein opening and quartz precipitation. At least veins 3 and 4 developed as conjugated arrays of stress-related primary tension gashes in sites of brittle failure. High values of $\delta^{18}O$ of 26‰ in veins 1 exceed the maximum values of 24‰ in the host rocks. This could be explained by a precipitation of quartz at fluid flowing down temperature. Additionally, as is indicated by fluid inclusions, CO_2 could have served as a source for ^{18}O. The fluids dissolved silica with initial high values of $\delta^{18}O$ from the ^{18}O-rich host rocks, probably biogenic metacherts, and the CO_2 could have been generated from interlayered graphitic metasediments.

Lower values of $\delta^{18}O$ in younger vein generations coincide with lower salinities and the presence of CH_4 in the fluid. This could be due to an increasing amount of isotopically light meteoric water and a change from oxidizing to reducing conditions in the fluid system. Furthermore, during precipitation of veins 4, the fluid system apparently changed from lithostatic to hydrostatic conditions as can be interpreted from distribution of fluid inclusion T_h and low densities.

A decrease of $\delta^{18}O$ in the range of 1–2‰ is observed from the margins to the centers of syntaxially crystallized single veins. When interpreted as a consequence of a changing fluid composition, this provides an argument for a comparably long-lasting time span (in the range of 10^3–10^6 years according to Fisher and Brantley (1992)) for precipitation of a single vein filling. Accordingly, the corresponding time span covered by the four vein generations that recorded marked changes of the fluid composition then should be in the range of several millions of years.

Quartz recrystallized in the veins 1 and 2 during shearing, fracturing and folding. Changes of initial isotopic compositions due to quartz recrystallization are difficult to assess. Domains with quartz subgrain rotation recrystallization along planar microfractures and former briquette structures conserve initial isotopic compositions. Grain boundary migration recrystallization led to isotopic homogenization in the vein. However, larger domains of quartz with small grain size in veins 1 are characterized by lower $\delta^{18}O$, which indicates the presence of 'new' quartz. Whatever, many studies consider an in-situ and chemically conservative deformation and recrystallization of quartz in veins and quartz-rich layers. Oxygen isotopes sensitively record quartz recrystallization and invasion in dependence on the fluid access. By small-scale isotopic studies in such veins and layers it is possible to recognize participation of changing fluid compositions and to identify the domains of invasion and precipitation of new quartz during a deformation.

The millimeter- to centimeter-scale oxygen isotope variations and the changing fluid compositions in the veins point to a small-scale and locally hosted limited H_2O–CO_2–NaCl fluid system. Apparently, the isotopic compositions in the fluid system were mainly controlled and buffered by the microquartzitic and graphitic host rocks, which are peculiar in the silicic volcano-detrital sequence of Belle-Ile. However, the changing fluid composition toward lower salinities and lower $\delta^{18}O$ in later veins indicates a limited but increasing contribution of meteoric water over the course of time. At a late stage of the evolution, this compositional change of the fluid system is accompanied by a change from lithostatic to hydrostatic pressure conditions. In conclusion, at Bordardoué in Belle-Ile we are dealing with a limited fluid system during progressive vein formation by four major fracturing stages. This is in marked contrast to large crustal scale and hydrothermally driven fluid systems with high quantities of externally derived fluids, described from other regions.

Acknowledgements

Oxygen isotope analyses performed by BS at the Institut de Minéralogie de l'Université de Lausanne, were made possible and accompanied by Z. Sharp, D. Kirschner and J. Hunziker. H.-P. Meyer and H. Remy assisted during the microprobe analyses at Mineralogisches Institut Heidelberg and Laboratoire de Pétrologie Minéralogique, Paris. A. Roostai, Institut für Geologie und Mineralogie, Erlangen, Germany, helped with the XRF analyses. The cathodoluminescence microscopy of the samples was possible by the help of J. Götze, Institute of Mineralogy TU Bergakademie Freiberg/Sachsen. An introduction of BS into fluid inclusion analysis was given by S. Uhlig, Freiberg. The manuscript was critically studied by T. Graupner, Würzburg. Encouraging and constructive reviews by P.D. Bons and an anonymous colleague helped us very much to understand the complexity of the Bordardoué veins. The project was financed by research grants (Schu 676/6-1, Schu 676/8-1) to BS from the Deutsche Forschungsgemeinschaft.

References

Audren, C., 1984. Lithostratigraphie et structure des séries volcano-sedimentaires de Belle-Ile-en-Mer Bretagne méridionale. Bulletin Societé géologique minéralogique de la Bretagne 16 (1), 31–44.

Audren, C., 1987. Évolution structurale de la Bretagne Méridionale au Palaeozoique. Mémoirs Societé géologique minéralogique de la Bretagne 31, 365pp, Rennes.

Audren, C., Plaine, J., 1986. Notice explicative de la feuille Belle-Ile-en-Mer et Iles Houat et Hoedic (Carte Géologique de la France 1:50,000). Éditions du B.R.G.M., 38pp, Orléans.

Audren, C., Gorre, G., 1995. Analyse géométrique de la propagation des plis dans un milieu naturel stratifié à fort contraste de compétence au cours d'un cisaillement simple. Comptes Rendues Académie Sciences Paris 320 (II), 609–616.

Audren, C., Triboulet, C., Chauris, L., Lefort, J.-P., Vigneresse, J.L., Audrain, J., Thiéblemont, D., Goyallon, J., Jégouzo, P., Guennoc, P., Augris, C., Carn, A., 1993. Note explicative de la feuille Ile de Groix (Carte Géologique de la France 1:25,000). Éditions du B.R.G.M., 101pp., Orléans.

Bakker, R.J., Jansen, B.H., 1990. Preferential water leakage from fluid inclusion by means of mobile dislocations. Nature 345, 58–60.

Bons, P.D., 2000. The formation of veins and their microstructures. In: Jessell, M.W. Urai, J.L. (Eds.), Stress, Strain and Structure. A volume in honour of W.D. Means. Journal of the Virtual Explorer (on-line) 2, http://virtualexplorer.com.au/VEjournal/Volume2/www/contribs/bons/index.html

Bons, P.D., Jessell, M.W., 1999. Micro-shear zones in experimentally deformed octachlorpropane. Journal of Structural Geology 21, 323–334.

Brown, P.E., 1989. FLINCOR: a fluid inclusion data reduction and exploration program. 2nd Biennial Pan-American Conference on Research on Fluid Inclusions (PACROFI). Program with Abstracts, p. 14.

Brown, P.E., 1998. Fluid inclusion modelling for hydrothermal systems. In: McKibben, M.A. Shanks, W.C. (Eds.), Applications of Microanalytical Techniques to Understanding Mineralizing Processes. Reviews in Economic Geology 7, pp. 151–171.

Brown, P.E., Lamb, W.M., 1986. Mixing of H_2O–CO_2 in fluid inclusions; geobarometry and Archean gold deposits. Geochimica Cosmochimica Acta 50, 847–852.

Brown, P.E., Lamb, W.M., 1989. P–V–T properties of fluids in the system H_2O–CO_2–NaCl: new graphical presentations and implications for fluid inclusion studies. Geochimica Cosmochimica Acta 53, 1209–1221.

Bucher, K., Frey, M., 1994. Petrogenesis of Metamorphic Rocks. Springer, Berlin, Heidelberg, New York.

Cipriani, C., Sassi, F.P., Scolari, A., 1971. Metamorphic white micas: definition of paragenetic fields. Swiss Bulletin of Mineralogy and Petrology 51, 259–302.

Cox, S.F., Etheridge, M.A., 1983. Crack-seal fibre growth mechanisms and their significance in the development of oriented layer silicate microstructures. Tectonophysics 92, 147–170.

Cox, S.F., Etheridge, M.A., 1989. Coupled grain-scale dilatancy and mass transfer during deformation at high fluid pressures: examples from Mount Lyell, Tasmania. Journal of Structural Geology 11, 147–162.

Diamond, L.W., 1994. Introduction to phase relations of CO_2–H_2O fluid inclusions. In: De Vivo, B., Frezzotti, M.L. (Eds.). Fluid Inclusions in Minerals: Methods and Applications. Virginia Polytechnic Institute and State University Press, pp. 131–158.

Dipple, G.M., Ferry, J.M., 1992a. Fluid flow and stable isotope alteration in rocks at elevated temperatures with applications to metamorphism. Geochimica Cosmochimica Acta 56, 3539–3550.

Dipple, G.M., Ferry, J.M., 1992b. Metasomatism and fluid flow in ductile fault zones. Contributions to Mineralogy and Petrology 112, 149–164.

Drury, M.R., Urai, J.L., 1990. Deformation-related recrystallization processes. Tectonophysics 172, 235–253.

Ferry, J.M., 1992. Regional metamorphism of the Waits River Formation, Eastern Vermont: delineation of a new type of giant metamorphic hydrothermal system. Journal of Petrology 33, 45–94.

Fisher, D., Byrne, T., 1990. The character and distribution of mineralized fractures in the Kodiak Formation, Alaska: implications for fluid flow in an underthrust sequence. Journal of Geophysical Research 95, 9069–9080.

Fisher, D., Brantley, S.L., 1992. Models of quartz overgrowth and vein formation: deformation and episodic fluid flow in an ancient subduction zone. Journal of Geophysical Research 97, 20043–20061.

Fourcade, S., Marquer, D., Javoy, M., 1989. $^{18}O/^{16}O$ variations and fluid circulation in a deep shear zone: the case of the Alpine ultramylonites from the Aar Massif (Central Alps, Switzerland). Chemical Geology 77, 119–131.

Fournier, R.O., 1985. The behaviour of silica in hydrothermal solutions. In: Berger, B.R., Bethge, P.M. (Eds.). Reviews in Economic Geology, Vol. 2, pp. 45–62. Geology and Geochemistry of Epithermal Systems.

Friedman, I., O'Neil, J.R., 1977. Compilation of stable isotope fractionation factors of geochemical interest. In: Fleischer, M. (Ed.), Data of Geochemistry, Chapter KK, 6th Ed. US Geological Survey Professional Paper 440KK.

Goldstein, R.H., Reynolds, T.J., 1994. Systematics of fluid inclusions in diagenetic minerals. SEPM Short Course 31, 1–199, Tulsa.

Götze, J., 1996. Kathodolumineszenz von Quarz—Grundlagen und Anwendung in den Geowissenschaften. Aufschluss 47, 215–223.

Götze, J., 1998. Principle and advantages of cathodoluminescence microscopy. Microscopy and Analysis 09/1998, 17–19.

Green, N.L., Usdansky, S.I., 1986. Toward a practical plagioclase–muscovite thermometer. American Mineralogist 71, 1109–1117.

Hall, D.L., Wheeler, J.R., 1992. Fluid composition and the decrepitation behaviour of synthetic fluid inclusions in quartz. 4th Biennial Pan-American Conference on Research on Fluid Inclusions (PACROFI). Program with Abstracts, p. 39.

Henderson, I.H.C., McCaig, A.M., 1996. Fluid pressure and salinity variations in shear-zone related veins, central Pyrenees, France: implications for the fault-valve model. Tectonophysics 262, 321–348.

Hoefs, J., 1997. Stable Isotope Geochemistry. Springer, Berlin, Heidelberg, New York.

Hoernes, S., Hoffer, E., 1985. Stable isotope evidence for fluid-present and fluid-absent metamorphism in metapelites from the Damara orogen, Namibia. Contributions to Mineralogy and Petrology 90, 322–330.

Kerrich, R., 1986. Fluid transport in lineaments. Royal Society London Philosophical Transactions A 317, 219–251.

Kirschner, D.L., Sharp, Z.D., Teyssier, C., 1993. Vein growth mechanisms and fluid sources revealed by oxygen isotope laser microprobe. Geology 21, 85–88.

Kirschner, D.L., Teyssier, C., Gregory, R.T., Sharp, Z.D., 1995. Effect of deformation on oxygen isotope exchange in the Heavitree Quartzite, Ruby Gap duplex, central Australia. Journal of Structural Geology 17, 1407–1423.

Laird, J., Albee, A.L., 1981. Pressure, temperature, and time indicators in mafic schists: their application to reconstructing the polymetamorphic history of Vermont. American Journal of Science 281, 127–175.

Massonne, H.-J., 1995. Thermodynamic properties of micas on the basis of high-pressure experiments in the systems K_2O–MgO–Al_2O_3–SiO_2–H_2O and K_2O–FeO–Al_2O_3–SiO_2–H_2O. Bochumer geologische und geotechnische Arbeiten 44, 109–113.

Massonne, H.-J., Schreyer, W., 1987. Phengite geobarometry based on the limiting assemblage with K-feldspar, phlogopite and quartz. Contributions to Mineralogy and Petrology 96, 212–224.

Matsuhisa, Y., Goldsmith, J.R., Clayton, R.N., 1979. Oxygen isotope fractionation in the systems quartz–albite–anorthite–water. Geochimica Cosmochimica Acta 43, 1131–1140.

Oliver, N.H.S., 1996. Review and classification of structural controls on fluid flow during regional metamorphism. Journal of Metamorphic Geology 14, 477–492.

Oliver, N.H.S., Cartwright, I., Wall, V.J., Golding, S.D., 1993. The stable isotope signature of kilometre-scale fracture-dominated metamorphic fluid pathways, Mary Kathleen, Australia. Journal of Metamorphic Geology 11, 705–720.

O'Hara, K., Haak, A., 1992. A fluid inclusion study of fluid pressure and salinity variations in the footwall of the Rector Branch thrust, North Carolina, USA. Journal of Structural Geology 14, 579–589.

O'Neil, J.R., 1986. Terminology and standards. In: Valley, J.W., Taylor,

H.P. Jr., O'Neil, J.R. (Eds.), Stable Isotopes in High Temperature Geological Processes. Reviews in Mineralogy 16, pp. 561–570.

Passchier, C.W., Trouw, R.A.J., 1996. Microtectonics. Springer, Berlin, Heidelberg, New York.

Ramsay, J.G., 1980. The crack-seal mechanism of rock deformation. Nature 284, 135–139.

Ramsay, J.G., Huber, M., 1983. The Techniques of Modern Structural Geology. Volume 1: Strain Analysis. Academic Press, London.

Ramseyer, K., Baumann, J., Matter, A., Mullis, J., 1988. Cathodoluminescence colours of alpha-quartz. Mineralogical Magazine 52, 669–677.

Rickard, M.J., Rixon, L.K., 1983. Stress configuration in conjugate quartz-vein arrays. Journal of Structural Geology 5, 573–578.

Roedder, E., 1984. Fluid inclusions. Reviews in Mineralogy 12, 1–646.

Rumble III, D., 1977. Mineralogy, petrology and oxygen isotope geochemistry of the Clough Formation, Black Mountain, Western New Hampshire, USA. Journal of Petrology 19, 317–340.

Rumble III, D., 1994. Water circulation in metamorphism. Journal of Geophysical Research 99, 15499–15502.

Rye, D.M., Bradbury, H.J., 1988. Fluid flow in the crust: an example from a Pyrenean thrust ramp. American Journal of Science 188, 197–235.

Secor, D.T., Pollard, D.D., 1975. On the stability of open hydraulic fractures in the earth crust. Geophysical Research Letters 2, 510–513.

Sharp, Z.D., 1992. In situ laser microprobe techniques for stable isotope analysis. Chemical Geology (Isotope Geoscience Section) 101, 3–19.

Sharp, Z.D., 1995. Oxygen isotope geochemistry of the Al_2SiO_5 polymorphs. American Journal of Science 295, 1058–1076.

Sibson, R.H., Moore, R.M., Rankin, A.H., 1975. Seismic pumping—a hydrothermal transport mechanism. Journal of the Geological Society London 131, 653–659.

Slater, D.J., Yardley, B.W.D., Spiro, B., Knipe, J., 1994. Incipient metamorphism and deformation in the Variscides of SW Dyfed, Wales: first steps towards isotopic equilibrium. Journal of Metamorphic Geology 12, 237–248.

Sterner, S.M., Bodnar, J.R., 1989. Synthetic fluid inclusions—VII. Re-equilibration of fluid inclusions in quartz during laboratory-simulated metamorphic burial and uplift. Journal of Metamorphic Geology 7, 243–260.

Stöckhert, B., Brix, M., Kleinschrodt, R., Hurford, A., Wirth, R., 1999. Thermochronometry and microstructures of quartz—a comparison with experimental flow laws and predictions on the temperature of the brittle-plastic transition. Journal of Structural Geology 21, 351–369.

Valley, J.W., 1986. Stable isotope geochemistry of metamorphic rocks. In: Valley, J.W., Taylor, H.P. Jr., O'Neil, J.R. (Eds.), Stable Isotopes in High Temperature Geological Processes. Reviews in Mineralogy 16, pp. 445–481.

Van Daalen, M., Heilbronner, R., Kunze, K., 1999. Orientation analysis of localized shear deformation in quartz fibres at the brittle-ductile transition. Tectonophysics 303, 83–107.

Velde, B., 1967. Si^{4+} contents of natural phengites. Contributions to Mineralogy and Petrology 14, 250–258.

Vityk, M.O., Bodnar, R.J., 1995. Do fluid inclusions in high-grade metamorphic terranes preserve peak metamorphic density during retrograde decompression?. American Mineralogist 80, 641–644.

Yardley, B.W.D., Bottrell, S.H., 1992. Silica mobility and fluid movement during metamorphism of the Connemara Schists, Ireland. Journal of Metamorphic Geology 10, 453–464.

Zhang, Y., Frantz, J.D., 1987. Determination of the homogenization temperatures and densities of supercritical fluids in the system NaCl–KCl–$CaCl_2$–H_2O using synthetic fluid inclusions. Chemical Geology 64, 335–350.